

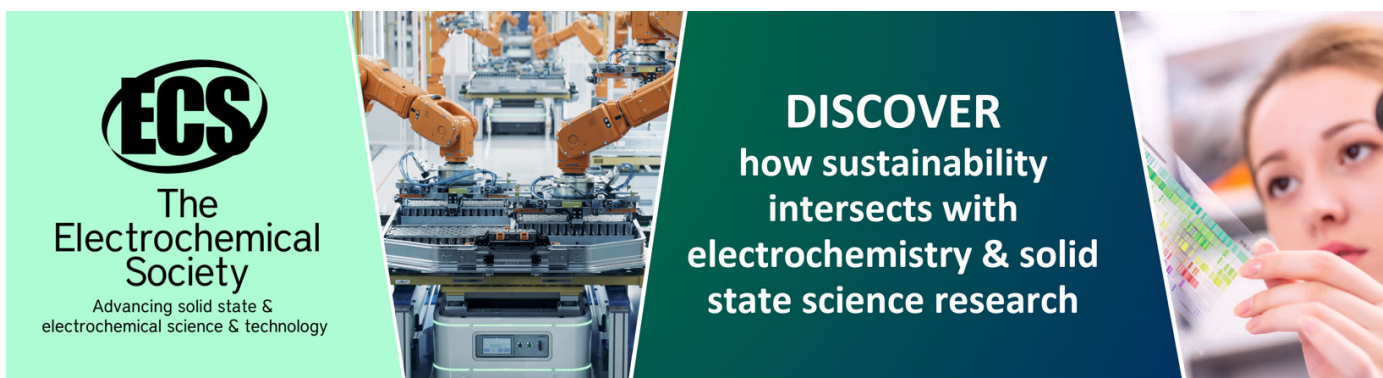
Experimental and numerical investigation of multipactor discharges in a coaxial waveguide

To cite this article: I A Kossyi *et al* 2010 *J. Phys. D: Appl. Phys.* **43** 345206

View the [article online](#) for updates and enhancements.

You may also like

- [Effects of rf magnetic field on upstream dielectric multipactor](#)
Huihui Wang, Dagang Liu, Laqun Liu *et al.*
- [Multipactor breakdown in microwave pulses](#)
J Rasch, D Anderson and V E Semenov
- [Application of energy-balance model from gas discharge to single-surface multipactor](#)
Huihui Wang, Xianchen Bai, Laqun Liu *et al.*



ECS
The
Electrochemical
Society
Advancing solid state &
electrochemical science & technology

DISCOVER
how sustainability
intersects with
electrochemistry & solid
state science research

Experimental and numerical investigation of multipactor discharges in a coaxial waveguide

I A Kossyi¹, G S Luk'yanchikov¹, V E Semenov², N A Zharova²,
D Anderson^{3,5}, M Lisak³ and J Puech⁴

¹ Prokhorov Institute of General Physics, Russian Academy of Sciences, 38 Vavilova Street, Moscow, 119991 Russia

² Institute of Applied Physics, Russian Academy of Sciences, 46 Ulyanov St., Nizhny Novgorod 603950, Russia

³ Department of Radio and Space Science, Chalmers University of Technology, 412 96 Goteborg, Sweden

⁴ Centre National d'Etudes Spatiales, 31401 Toulouse, France

E-mail: elfda@chalmers.se

Received 18 May 2010, in final form 14 July 2010

Published 12 August 2010

Online at stacks.iop.org/JPhysD/43/345206

Abstract

An experimental and numerical investigation is made of multipactor discharges in a coaxial waveguide. Particular attention is given to the determination of the multipactor threshold and the distribution of the impact energy of the electrons. Simulations are carried out for different parameters of the secondary emission coefficient of the electrode surfaces. This makes it possible to determine these parameters through a comparison between the numerical and experimental results. The comparison also shows that the observed multipactor is mainly of polyphase (non-resonant) nature and represents a mixture of single- and double-surface multipactor discharges.

1. Introduction

Multipactor discharges constitute a potentially severe problem for modern microwave systems involving high powers and operating close to vacuum conditions [1–7]. The multipactor phenomenon has been intensively studied experimentally, theoretically and numerically for more than 50 years [8–18]. However, comparisons between experimental and theoretical results present a difficult problem. On the one hand, multipactor experiments do not, in general, involve detailed measurements of the secondary emission properties of the solid surfaces which generate the multipactor electron avalanche. On the other hand, numerical results are usually obtained using a particular model for the secondary electron emission yield and the sensitivity of the concomitant results on this model is not clear. Some data on the secondary emission properties of different materials can be found in the ESA standard [19]. However, these data do not take into account the contamination of solid surfaces that is present in realistic experiments.

The secondary emission properties are known to be very sensitive to different surface contaminations and consequently the simulations which are carried out using standard emission data may deviate significantly from the experimental results [20]. However, the problem can be turned around in such a way that a comparison between numerical calculations and measurements is instead used to obtain information concerning the (unknown) parameters of the secondary emission yield.

The determination of the multipactor threshold is the most simple and common measurement in an experiment. In order to obtain a comprehensive comparison of these measurements with theory, it is necessary to know the dependence of the multipactor threshold on frequency and the geometrical parameters of the system [2, 21–24]. However, having access to additional experimental data (i.e. not only the multipactor threshold) and by carrying out numerical simulations within a wide range of parameters, it is possible to determine the parameters of the secondary emission yield even in the case of fixed system geometry and frequency. For example, in [20] such additional information was obtained by experimental investigation of multipactor discharges in a

⁵ Author to whom any correspondence should be addressed.

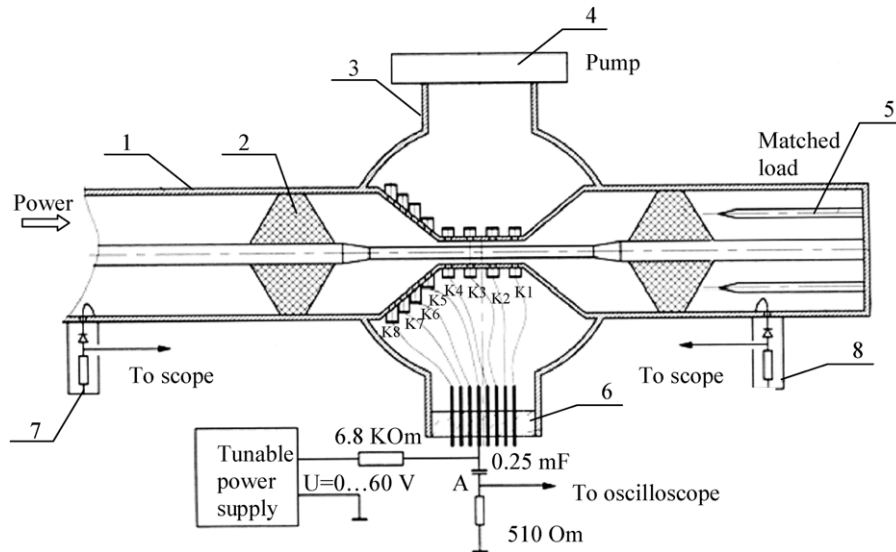


Figure 1. Scheme of the experimental setup: (1) coaxial waveguide, (2) fluoro-plastic windows, (3) vacuum chamber, (4) electric-discharge vacuum pump, (5) matched load, (6) multi-pin input for power supply of the collectors and (7, 8) microwave detectors. Collectors K_1 – K_8 record the electron/ion current depending on the dc bias applied.

rectangular waveguide within a wide range of transmitted microwave powers and by using independent measurements of the first cross-over energy of the secondary emission yield in the waveguide. In the present paper, multipactor breakdown in a coaxial transmission line is investigated experimentally and simulated numerically. The geometry of the coaxial line, as well as the microwave frequency, was kept fixed. In contrast to [20] it was not possible to measure the first cross-over energy in the waveguide. Instead the distribution of the impact energy of the multipacting electrons was measured in the experiment, as suggested in [24]. This information made it possible to do a comprehensive comparison with numerical simulations and was also used to confirm the polyphase nature of the multipactor discharge [25–29].

2. Experimental setup

A schematic picture of the experimental setup used for investigating the multipactor discharges in a coaxial cylindrical waveguide is shown in figure 1. The central section of the coaxial waveguide 1 with an outer electrode (made of brass) of radius $R_{out} = 12.5$ mm and an inner electrode (made of duralumin) of radius $R_{in} = 3$ mm is placed in the vacuum chamber 3. Within the chamber, the waveguide narrows linearly to the radii of $R_{out} = 4$ mm and $R_{in} = 2$ mm. The outer electrode has a set of holes for pumping out the waveguide and (in the case of a multipactor discharge) for extracting the electron current to the ring collectors K_1 – K_8 . The diameter of the holes was small enough (0.5 mm) to avoid significant perturbations of the electromagnetic field in the waveguide. Four collectors K_1 – K_4 are arranged along the narrowest cylindrical part of the waveguide (of length $L = 5$ cm), whereas the other K_5 – K_8 collectors are installed in its expanding conical part (more specifically in the cross-sections where the radius of the outer electrode equals 4.4 mm, 4.7 mm, 5.8 mm and 10.8 mm, respectively). The electric current from

the collectors was recorded using an oscilloscope (Tektronix TDS 220), which visualized the time evolution of the current. The potential bias between the collector and the outer electrode could be varied and the dependence of the collector current on this potential bias could be determined. Thus, information concerning the energy distribution of the impacting electrons [24] could be obtained. This made it possible to measure also the ionic current (if any) to the collectors and thereby to distinguish the electron multipactor effect from the plasma effect caused by microsparks [20, 27].

The fluoro-plastic windows 2 separated the central vacuum section of the waveguide in the chamber from the side sections, which were filled by air at atmospheric pressure. The right (edge) waveguide section was held at atmospheric pressure and equipped with the matched load 5 to realize the regime of a travelling electromagnetic wave in all sections of the coaxial line and to keep the power reflection coefficient very low (less than 0.25%). To reduce the possibility of the appearance of microsparks at the metal–dielectric interface [30, 31], the windows were positioned in the widest portion of the coaxial waveguide, where the microwave electric field is the weakest. Furthermore, to reduce the density of the plasma that can result from the microsparks, the joint between the window and the inner electrode was sealed by a narrow circular groove. The chamber and the waveguide are pumped out to a pressure of $(2-3) \times 10^{-6}$ Torr by the oil-free electric-discharge (titanium) pump 4. The fundamental mode in the coaxial line was excited at a frequency $f = 2.45$ GHz by a microwave generator (magnetron) that operated in the pulse repetition regime with pulse duration $\tau_f = 1$ ms, peak power $P \leq 3$ kW and repetition frequency $F = 0.4$ Hz. The detector heads 7 and 8 measure the microwave field intensity in the input and output sections of the waveguide. The field intensity in these sections depends on the wave reflection and the absorption that would be caused by a discharge in the waveguide. Therefore it was possible to identify such a discharge using signals from detectors 7 and 8.

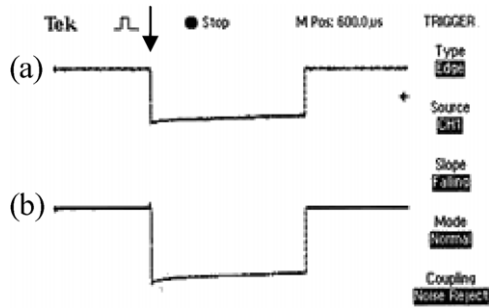


Figure 2. Representative pulse oscillograms from the detectors at the input (a) and output (b) sections of the vacuum chamber in the case of low input power ($P = 0.9$ kW) when there is no discharge in the coaxial waveguide. The vertical arrow \downarrow in the top line indicates the beginning of the microwave pulse.

3. Experimental results

Figures 2 and 3 present typical oscillograms of the signal obtained from the microwave detectors 7 and 8 in qualitatively different cases of microwave powers below and above the breakdown threshold. At low microwave powers ($P \leq 0.9$ kW), the signals from both detectors have a similar profile—a replica of the profile of the microwave pulse (see figure 2). However at higher power levels ($P \geq 1$ kW), the signal profiles are qualitatively different (figure 3) and demonstrate an abrupt jump (up or down) in the field intensity after a temporal delay that depends on the excess power above the threshold. In the input section, a sharp increase in the microwave field intensity is observed which can be understood as a result of constructive interference between the incident electromagnetic wave and the reflected electromagnetic wave that appears due to the presence of the discharge in the waveguide. At the same time the field intensity in the output section decreases as a result of both partial reflection and absorption of the incident wave.

The signals from collectors K_1 – K_8 present additional information on the discharge properties. At low microwave powers, the electric current from all collectors is zero during the pulse whereas at higher power levels current pulses are recorded from all collectors, although with slightly different time delays and different peak values (figure 3). The current profile is found to be qualitatively similar for all collectors. Typically it starts with a very short peak (with a duration of about 2–10 μ s) and is followed by a considerably slower increase in the current and the establishing of a certain quasi-stationary level. The first peak is associated with the electron multipactor discharge since no ionic current is detected during this time. The multipactor peaks are found to appear almost simultaneously at all collectors although the values are quite different (the highest peak amplitude is detected at the collector K_5 , as seen from figure 4)⁶. On the other hand, the delay of the second current peak is quite different for different collectors. These peaks and the quasi-stationary current are associated

⁶ The observed phenomena (the simultaneous formation of the first current peak at different collectors as well as the separation of the maximum current from the dielectric seal) confirm that the physical mechanism behind is not plasma jets generated by micro-sparks at the metal–dielectric interface, but rather due to multipactor discharges.

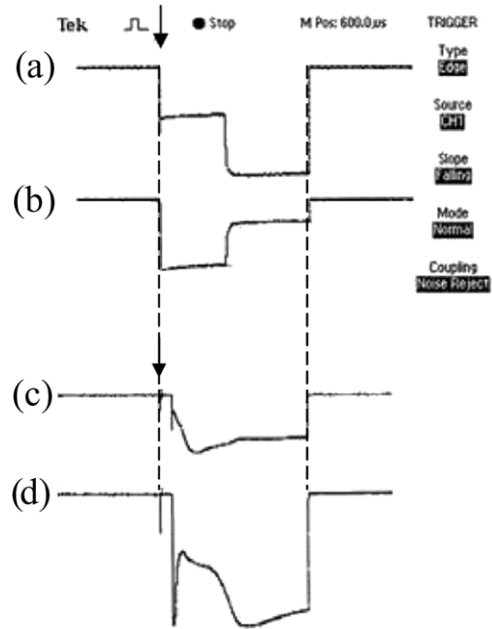


Figure 3. The same as in figure 2 but in the case of high input power ($P = 1.5$ kW) when there is a discharge in the coaxial waveguide. Lower part of figure shows representative oscillograms of the electron current signals from collectors K_8 (c) and K_5 (d). The vertical arrow \downarrow in the top line indicates the beginning of the microwave pulse.

with plasma formation due to ionization of gas desorption from the waveguide walls. An ionic current is detected at this stage when the negative potential bias between the collector and the outer coaxial electrode becomes strong enough to reflect all electrons. The electric current to the collector (if any) is then completely determined by ions. It should also be noted that perturbations of the signals from the microwave detectors (figures 2 and 3) are observed only after the plasma formation.

Figure 5 illustrates the dependence of the multipactor peak current on the bias voltage applied between collector K_4 and the outer electrode of the coaxial waveguide. The current–voltage characteristics make it possible to determine the distribution of the electron impact energy, W , at the outer electrode (figure 6). Note that $F(W) \propto dj_{ek}/dU_p$, where the impact energy is related to the potential as $W = -eU_p$. This distribution is found to be considerably different from that corresponding to a resonance multipactor discharge. In fact, resonance theory predicts a narrow peak in electron impact energy [32], whereas the measurements demonstrated a relatively wide spread of electron impact energy extending up to 60 eV. Figure 6 also shows the existence of a considerable fraction of electrons with small energy (less than 10 eV) that can only be due to electrons returning to the surface of emission without having experienced any significant acceleration by the microwave field.

4. Numerical simulations

Numerical simulations of the multipactor discharge in the coaxial line were carried out using the software COAXMUL which represents an upgrade of a previous version described

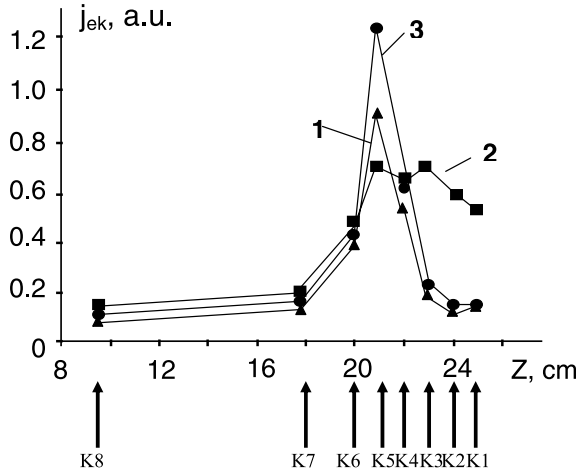


Figure 4. Peak value (arbitrary units) of the multipactor electron current for different microwave powers and positions of the collectors along the coaxial waveguide. Each indicated point corresponds to a particular collector from K_8 (the most left) up to K_1 (the most right). Curve 1 (triangles) corresponds to $P = 1$ kW; curve 2 (squares) to $P = 1.5$ kW and curve 3 (circles) to $P = 3$ kW.

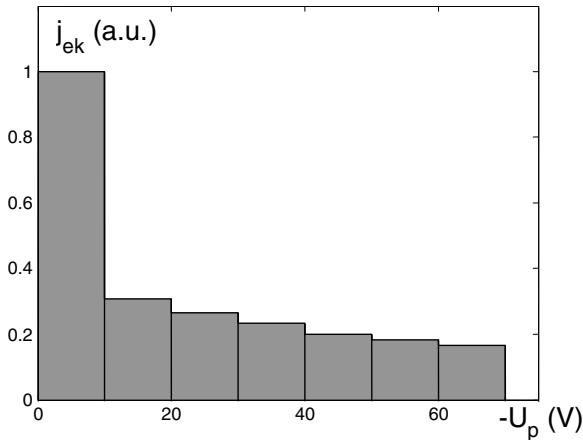


Figure 5. Electron current to collector K_4 (arbitrary units) versus electron decelerating potential $-U_p$ for $P = 1.5$ kW.

in [33]. The software is based on a PIC algorithm and considers the motion of macroparticles (subsequently named computer particles) which have the same charge-to-mass ratio as the electrons. The simulations are started by the launching of seed particles having stochastic initial velocities governed by a Maxwellian probability distribution. These particles move under the action of the electromagnetic field and release a number of secondary particles when they collide with the metal walls. The secondary emission is considered as a stochastic process with a probability distribution governed by the impact energy of the particles and chosen so as to correspond to Vaughan's approximation [34] for the average value of the secondary emission yield. The secondary particles are assumed to start with stochastic initial velocities governed by the same Maxwellian probability distribution as the seed particles.

In conventional PIC software, the charge and mass of the computer particles are fixed during the simulations whereas the number of particles varies. It should be emphasized

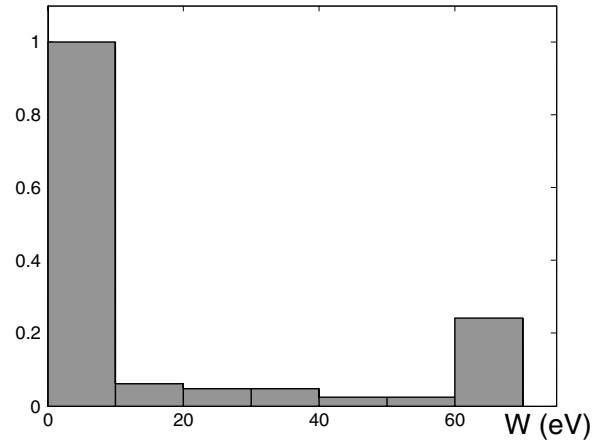


Figure 6. Distribution of electron impact energy obtained from the current–voltage characteristics shown in figure 5.

that using a small number of computer particles leads to considerable stochastic fluctuations in the results whereas a large number of computer particles require long simulation times. Therefore, it is difficult to simulate the long time evolution of the multipactor. To avoid this problem in the software COAXMUL, the charge and mass of the computer particles are not considered as fixed (only the ratio between these quantities is kept fixed). This makes it possible to keep the number of computer particles within a desirable range using the following prescription: when, during the course of the simulation, the number of computer particles exceeds some threshold value, N_{th} , the software randomly excludes one-half of these particles from further consideration and simultaneously doubles the charge and mass of the remaining particles. On the other hand, if the number of computer particles becomes less than $0.3N_{th}$, the software splits each computer particle into two new particles having one-half of the previous charge and mass. This procedure makes it possible to study the long time evolution of the multipactor avalanche while still having high simulation speed and accuracy.

It is important to note that the software uses the macroparticle mass and charge only to calculate the total electron number which is determined as the ratio of the total mass of all macroparticles to the mass of a single electron. The trajectory of each macroparticle is determined by its charge-to-mass ratio, and consequently this trajectory and also the impact velocity coincide completely with the trajectory and the impact velocity of a single electron. This means that any macroparticle can be treated as the corresponding number of electrons having the same coordinate and velocity. A collision of a macroparticle with a solid surface is treated as a collision of the corresponding number of electrons with this surface. This process is accompanied by a release of secondary electrons, the number of which is determined by the electron impact energy or by the impact velocity of the macroparticle. However, within the software the secondary electrons are again integrated into the macroparticles having the same mass and charge as the impacting macroparticle.

The first series of simulations was carried out to study the dependence of the initial stage of the multipactor avalanche

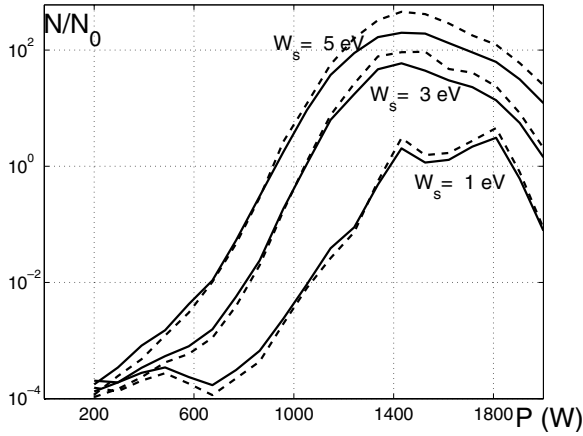


Figure 7. The dependence of the relative increase in the electron number, N/N_0 , after 100 microwave periods on the microwave power, P , and the properties of the secondary emission yield of the waveguide walls. All simulations were completed taking the same coaxial waveguide with electrode radii $R_{in} = 2$ mm, $R_{out} = 4$ mm, the same frequency 2.45 GHz and the same value of the first cross-over energy $W_1 = 20$ eV. Each curve represents results calculated for fixed maximum value of the secondary emission yield (the solid lines correspond to $\sigma_{max} = 2$, whereas the dotted lines correspond to $\sigma_{max} = 3$) and fixed value of the average initial energy, W_s , of emitted electrons (the chosen value is shown close to the lines).

on the secondary emission properties of the waveguide walls and the microwave power transmitted through the waveguide. The number of seed particles (having the conventional electron charge and mass) was taken to be $N_0 = 25\,000$ and these particles were launched from the surface of the inner electrode during the first microwave period. The inner and outer electrode radii were taken to be 2 mm and 4 mm, respectively, the microwave frequency was 2.45 GHz and the threshold value of the computer particles was $N_{th} = 50\,000$. In these simulations, the number of electrons, N , was recorded after 100 microwave periods and the relative increase in the electron number, N/N_0 , was plotted against the microwave power, P , for different combinations of parameters such as average initial energy of electrons, W_s , first cross-over point, W_1 , and maximum value, σ_{max} , of the secondary emission curve. The results (figures 7 and 8) demonstrate that the threshold power for the multipactor avalanche (which corresponds to the equality $N/N_0 = 1$) is sensitive to the values of W_s and W_1 whereas its dependence on the value σ_{max} is less pronounced. On the other hand, figure 8 clearly illustrates that the threshold power, 900 W (the same as that observed in experiments), can be realized using considerably different combinations of parameters (for instance, $W_s = 1$ eV and $W_1 = 10$ eV or $W_s = 5$ eV and $W_1 = 20$ eV). The multipactor simulations were repeated for these parameter combinations, but using a larger value of N_{th} ($N_{th} = 2 \times 10^5$) and studying the temporal evolution of the electron number, the power deposition on the electrode surface and the impact electron energy. The microwave power was taken to be 1.5 kW in these simulations which were aimed at determining the distribution of the electron impact energy. At this high microwave power, the growth of the multipactor avalanche was faster in the case

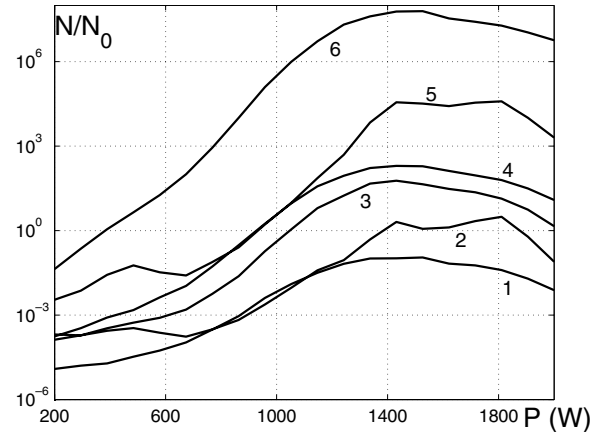


Figure 8. The same as in figure 7, but taking $\sigma_{max} = 2$ for all curves and different combinations of W_1 and W_s . Line 1 corresponds to $W_1 = 30$ eV and $W_s = 5$ eV; line 2 to $W_1 = 20$ eV and $W_s = 1$ eV; line 3 to $W_1 = 20$ eV and $W_s = 3$ eV; line 4 to $W_1 = 20$ eV and $W_s = 5$ eV; line 5 to $W_1 = 10$ eV and $W_s = 1$ eV; line 6 to $W_1 = 10$ eV and $W_s = 5$ eV.

of $W_s = 1$ and $W_1 = 10$ eV (figure 9). The evolution of the impact electron energy shows a sequence of peaks, shifted with respect to each other at the inner and outer electrodes. The amplitudes of the peaks in impact energy are similar in both cases (figure 10). However, one can clearly see that in the first case ($W_s = 1$ and $W_1 = 10$ eV), the duration of the impact energy peaks is shorter and their amplitude is higher at the outer electrode. The difference between the two cases becomes more pronounced when the time evolution of the heating power at both electrodes is studied (figure 11). In the simulations the relative heating power was calculated as follows. During each temporal interval equal to 0.05 of the microwave period, all impact energies at each electrode were summarized: $W_{\Sigma} = \sum W_i$. During the same temporal interval all initial energies of the secondary electrons were also summarized: $W_{0\Sigma} = \sum W_{0i}$. The relative heating power (during the considered temporal interval), Q , was then calculated as $Q = 20(W_{\Sigma} - W_{0\Sigma})/(NT)$, where N is the number of electrons in the middle of the considered temporal interval and T denotes the microwave period. Specifically, in the first case electrons collide with the outer electrode more often and thereby the heating power is considerably higher there than at the inner electrode. The same asymmetry between the outer and inner electrode is observed also in the second case, but the difference in the heating power is not so pronounced in this case. Detailed simulations were also used to calculate the distribution of electron impact energy at the outer electrode (figure 12). In both cases considered, the numerical results demonstrate the presence of a considerable fraction of electrons with low impact energy, in agreement with the measurements (cf figure 6). Also in both cases, no electron impact energies greater than 80 eV were found. However, in contrast to the experiment, the fraction of electrons with impact energies between 20 and 60 eV was found to be very small in the first case whereas in the second case this fraction was found to be in reasonable agreement with the measurements.

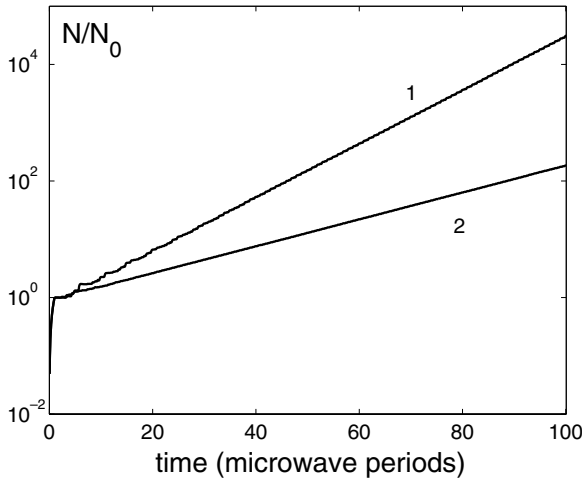


Figure 9. The evolution of the relative number of electrons at high microwave power, $P = 1.5$ kW and for different parameters of the secondary electron emission yield. Line 1 corresponds to $\sigma_{\max} = 2$, $W_1 = 10$ eV and $W_s = 1$ eV and line 2 to $\sigma_{\max} = 2$, $W_1 = 20$ eV and $W_s = 5$ eV.

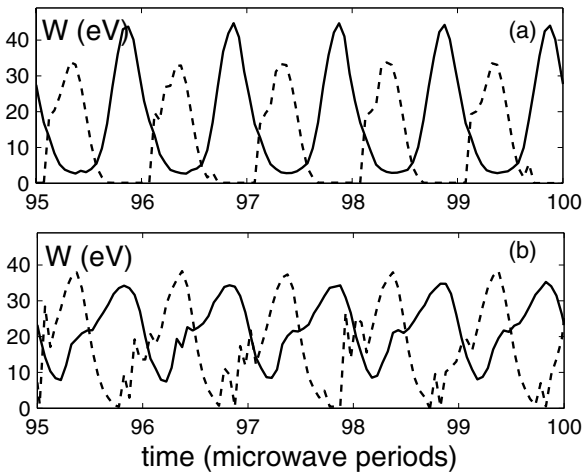


Figure 10. The evolution of impact electron energy, W (averaged over a time interval equal to 0.05 microwave periods), at high microwave power $P = 1.5$ kW and for different parameters of the secondary electron emission yield ((a) corresponds to $\sigma_{\max} = 2$, $W_1 = 10$ eV and $W_s = 1$ eV and (b) to $\sigma_{\max} = 2$, $W_1 = 20$ eV and $W_s = 5$ eV). The solid line represents the electron impact energy at the outer electrode, whereas the dotted line represents the impact energy at the inner electrode.

5. Discussion

In general, the multipactor phenomenon is discussed in terms of resonance between the oscillations of the electrons and the rf electric field in the device volume [8, 11, 32]. When resonance theory is used to analyse multipactor breakdown in a coaxial line [23, 35], it predicts growth of an electron avalanche only within relatively narrow separated bands of transmitted power. However, these predictions are not in agreement with our experiments where the multipactor was observed within a wide range of powers in agreement with the predictions of the polyphase multipactor theory [25–29]. One important reason for this discrepancy is the spread of initial

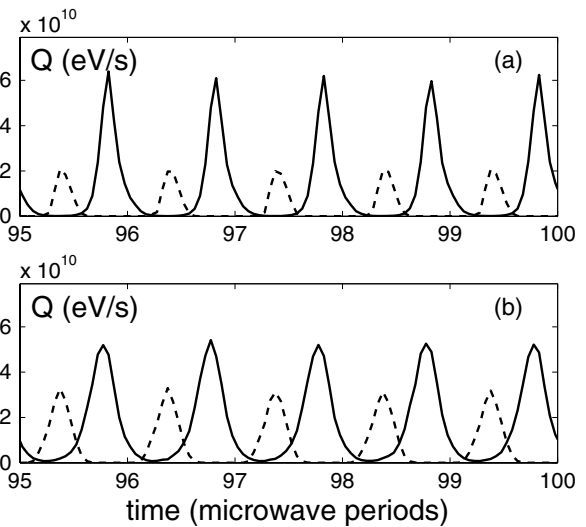


Figure 11. The evolution of heating power, Q , per multipacting electron (averaged over a time interval equal to 0.05 microwave periods) at high microwave power $P = 1.5$ kW and for different parameters of the secondary electron emission yield ((a) corresponds to $\sigma_{\max} = 2$, $W_1 = 11$ eV and $W_s = 1$ eV and (b) to $\sigma_{\max} = 2$, $W_1 = 20$ eV and $W_s = 5$ eV). The solid line represents the heating power at the outer electrode, whereas the dotted line represents the heating power at the inner electrode.

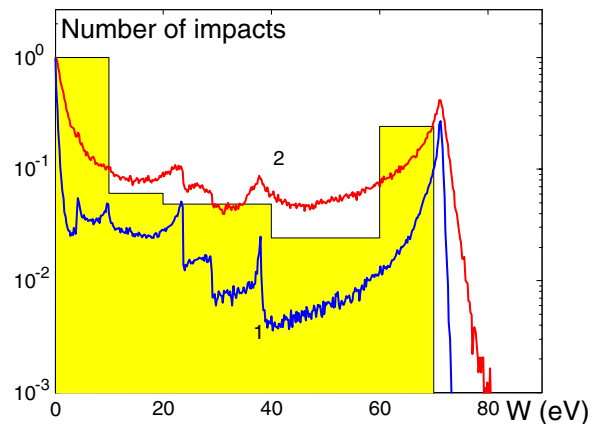


Figure 12. The distribution of electron impact energy at the outer electrode (normalized to the maximum value). The presented results are averaged over the last 8 (i.e. from 92 up to 100) microwave periods. The simulations are carried out using the same parameters as in figures 10 and 11. Line 1 corresponds to $\sigma_{\max} = 2$, $W_1 = 11$ eV and $W_s = 1$ eV and line 2 to $\sigma_{\max} = 2$, $W_1 = 20$ eV and $W_s = 5$ eV). Superimposed are the experimental results presented in figure 6. (This figure is in colour only in the electronic version)

electron emission velocity, which is not negligible compared with the impact velocity corresponding to the first cross-over point of the secondary emission curve. This statement is confirmed by the results of the numerical simulations. Actually, figure 7 demonstrates that separated narrow peaks (not very well pronounced) in the dependence of the relative number of electrons on microwave power appear only in the case of small initial energy, W_s , of the secondary electrons. (Note that W_s is directly proportional to the square of the electron velocity spread in the case of a Maxwellian probability

distribution.) Another argument for the polyphase nature of the observed multipactor process is the wide distribution of electron impact velocities found both in measurements and in simulations (figures 6 and 12). It should be emphasized that the strong periodic pulsations in electron impact energy and heating power (figures 10 and 11) are also in agreement with the polyphase theory [27], which predicts that the probability of electron collisions with the walls oscillates with a phase shift of $\pi/2$ with respect to the microwave field oscillations.

At first sight a serious argument against the polyphase nature of the multipactor seems to be the fact that the numerical simulations indicate a considerable influence of the electron initial energy on the multipactor threshold. When applied to the plane-parallel model, the polyphase theory [27] does not predict such an effect since the contribution of the electron initial energy to the impact energy is relatively weak. However, the situation changes drastically when the multipactor occurs in a coaxial waveguide. As found in previous studies [23, 35, 36], depending on parameters, two qualitatively different regimes of multipactor (two-sided and one-sided) are possible in a coaxial waveguide. Specifically, when the initial electron velocity is neglected and the ratio of outer to inner radii exceeds $\sqrt{3}$, theory predicts that only one-sided multipactor (localized at the outer electrode) is possible [35]. This result is caused by the action of the Miller (or ponderomotive) force which tends to push electrons out of regions with strong rf field (here the vicinity of the inner electrode). Clearly, a finite initial velocity makes it possible for an electron to overcome the Miller repulsion and shifts the border between the two-sided and one-sided multipactor regimes towards higher values of $R_{\text{out}}/R_{\text{in}}$. In our experiments, this ratio was taken as $R_{\text{out}}/R_{\text{in}} = 2$ and consequently an increase in electron energy from 1 up to 5 eV corresponds to a transition from a multipactor which is mainly one-sided to one that is mainly two-sided. This conclusion is confirmed by numerical simulations (cf figure 11) and makes it possible to understand why the multipactor threshold is so sensitive to electron initial energy.

In order to understand the observed distribution of electron impact velocities, we emphasize the following points:

- (i) A spread of electron initial velocity results in a considerable spread of the corresponding flight times and therefore an important part of the electron impacts at 'wrong' phases of the microwave field, i.e. at moments when this field does not accelerate secondary electrons out from the surface of emission, but instead pushes them back to this surface. Such secondary electrons return in a short time with an energy close to their initial energy and contribute to the peak of low energy electron impacts (figure 12). The low energy peak contains approximately half of all impacts whereas its width is about the average initial energy of the secondary electrons.
- (ii) When a secondary electron starts from the outer electrode and returns to this electrode, its maximum impact energy is $2mV_{\omega}^2$ [35], where $V_{\omega}eE/m\omega$ is the electron oscillatory velocity at the outer electrode (e and m denote electron charge and mass, respectively, ω is the circular field frequency and E denotes the electric field amplitude at the outer electrode). At the input power, $P = 1.5$ kW, the maximum impact energy of returning electrons is estimated to be $2mV_{\omega}^2 \approx 24$ eV, which corresponds to one of the intermediate peaks in figure 12.
- (iii) When a secondary electron starts from the inner electrode and then collides with the outer electrode, its maximum impact energy can also be estimated using the approximate theory of electron motion in a coaxial waveguide [35] with the result $mV_{\omega}^2(1 + \sqrt{5.5})^2/2 \approx 67$ eV, which corresponds to the peak with a high impact energy in figure 12.

The above simple analysis implies that the contribution to the multipactor avalanche from electrons which transit between the electrodes is important even in the considered case of small initial energy of the electrons.

6. Conclusion

An experimental study and numerical simulations have been carried out for a multipactor discharge in a coaxial waveguide in vacuum and the obtained results have been analysed and compared. This comparison makes it possible to determine the parameters of the secondary emission yield of the waveguide walls in the experiment. It is also possible to conclude that the multipactor discharge observed in the experiment is excited in the polyphase regime and that both one-sided and two-sided multipactor avalanches contribute to the discharge.

Acknowledgments

This work was supported in part by the Russian Foundation for Basic Research through grant number 09-02-97024.

References

- [1] Ikeda Y, Imai T and Sakamoto K 1989 Discharge at the pillbox window for an LHRF launcher *IEEE Trans. Plasma Sci.* **17** 534–40
- [2] Woode A and Petit J 1990 Investigations into multipactor breakdown in satellite microwave payloads *ESA J.* **14** 467–78
- [3] Rozario N, Lenzing H F, Reardon K F, Zarro M S and Baran C G 1994 Investigation of Telstar 4 spacecraft Ku-band and C-band antenna components for multipactor breakdown *IEEE Trans. Microw. Theory Techn.* **42** 558–64
- [4] Kovalev N F, Nechaev V E, Petelin M I and Zaitsev N I 1998 Scenario for output pulse shortening in microwave generators driven by relativistic electron beams *IEEE Trans. Plasma Sci.* **36** 246–51
- [5] Neuber A, Dickens J, Hemmert D, Krompholz H, Hatfield L L and Kristiansen M 1998 Window breakdown caused by high-power microwaves *IEEE Trans. Plasma Sci.* **26** 296–303
- [6] Power J G, Gai W, Gold S H, Kinkead A K, Konecny R, Jing C, Liu W and Yusof Z 2004 Observation of multipactor in an alumina-based dielectric-loaded accelerating structure *Phys. Rev. Lett.* **92** 164801
- [7] Abe T, Kageyama T, Akai K, Ebihara K, Sakai H and Takeuchi Y 2006 Multipactoring zone map of an rf input coupler and its application to high beam current storage rings *Phys. Rev. Spec. Top.-Accel. Beams* **9** 062002

- [8] Vaughan J R M 1988 Multipactor *IEEE Trans. Electron Devices* **35** 1172–80
- [9] Kishek R A, Lau Y Y, Ang L K, Valfells A and Gilgenbach R M 1998 Multipactor discharge on metal and dielectrics: Historical review and recent theories *Phys. Plasmas* **5** 2120–6
- [10] Nagesh S K, Revannasiddiah D and Shastry S V K 2005 Investigation of multipactor breakdown in communication satellite microwave co-axial systems *PRAMANA—J. Phys.* **64** 95–110
- [11] de Lara J, Perez F, Alfonso M, Galan L, Montero I, Roman E and Raboso D 2006 Multipactor prediction for on-board spacecraft RF equipment with the MEST software tool *IEEE Trans. Plasma Sci.* **34** 476–84
- [12] Perez M, Tienda C, Vicente C, Coves A, Torregrosa G, Gimeno B, Barcot R, Boria V E and Raboso D 2006 Multipactor analysis in coaxial waveguides for satellite applications using frequency-domain methods 2006 *IEEE MTT-S International Microwave Symposium Digest (San Francisco, CA)* (IEEE Cat. No. 06CH37734C) pp 1045–8
- [13] Yu M 2007 Power-handling capability for rf filters *IEEE Microw. Mag.* **8** 88–97
- [14] Gusarova M A, Kaminsky V I, Kravchuk L V, Kutsaev S V, Lalayan M V, Sobenin N P and Tarasov S G 2009 Multipacting simulation in accelerating RF structures *Nucl. Instrum. Methods Phys. Res. A* **599** 100–5
- [15] Sinityn O V, Nusinovich G S and Antonsen T M Jr 2009 Self-consistent nonstationary two-dimensional model of multipactor in dielectric-loaded accelerator structures *Phys. Plasmas* **16** 073102
- [16] Perez A M, Boria V E, Gimeno B, Anza S, Vicente C and Gil J 2009 Multipactor analysis in circular waveguides *J. Electromagn. Waves Appl.* **23** 1575–83
- [17] Semenov V E, Rakova E I, Sazontov A G, Nefedov I M, Pozdnyakova V I, Shereshevskii I A, Anderson D, Lisak M and Puech J 2009 Simulations of multipactor thresholds in shielded microstrip lines *J. Phys. D: Appl. Phys.* **42** 205204
- [18] Perez A M, Tienda C, Vicente C, Anza S, Gil J, Gimeno B, Boria V E and Raboso D 2009 Prediction of multipactor breakdown thresholds in coaxial transmission lines for travelling, standing and mixed waves *IEEE Trans. Plasma Sci.* **37** 2031–40
- [19] ESA for ECSS 2003 *Space Engineering, Multipactor Design, and Test* ESA Publications Division, Noordwijk, The Netherlands, ECSS-E-20-01-01A
- [20] Kossyi I A, Lukyanchikov G S, Semenov V E, Rakova E I, Anderson D, Lisak M and Puech J 2008 Polyphase (non-resonant) multipactor in rectangular waveguides *J. Phys. D: Appl. Phys.* **41** 065203
- [21] Woo R and Ishimaru A 1967 A similarity principle for multipacting discharges *J. Appl. Phys.* **38** 5240–4
- [22] Woo R 1968 Multipacting discharges between coaxial electrodes *J. Appl. Phys.* **39** 1528–33
- [23] Somersalo E, Yla-Oijala P and Proch D 1995 Analysis of multipacting in coaxial lines *Proc. 1995 Particle Accelerator Conf. (Dallas, TX)* (Cat. No 95CH35843) vol 3, pp 1500–2
- [24] Graves T P, LaBombard B, Wukitch S and Hutchinson I 2006 The coaxial multipactor experiment (CMX): a facility for investigating multipactor discharges *Rev. Sci. Instrum.* **77** 014701
- [25] Luk'yanchikov G S 1975 Multiphase uniform secondary-emission microwave discharge at a solid surface *Sov. Phys. Tech. Phys.* **19** 1196–9
- [26] Dorofeyuk A A, Kossyi I A, Luk'yanchikov G S and Savchenko M M 1976 Study of the electron discharge caused by the interaction of microwave radiation with metal surfaces *Sov. Phys. Tech. Phys.* **21** 76–80
- [27] Grishin L V, Dorofeyuk A A, Kossyi I A, Luk'yanchikov G S and Savchenko M M 1977 *A Study of Secondary-Emission Microwave Discharges with Large Electron Transit Angles (Lebedev Physics Institute Series vol 92)* (New York: Consultants Bureau) pp 63–101
- [28] Grishin L V and Luk'yanchikov G S 1976 Multipactor discharge with an electron velocity distribution *Sov. Phys. Tech. Phys.* **21** 307–11
- [29] Sazontov A, Buyanova M, Semenov V, Rakova E, Vdovicheva V, Anderson D, Lisak M, Puech J and Lapiere L 2005 Effect of emission velocity spread of secondary electrons in two-sided multipactor *Phys. Plasmas* **12** 053102
- [30] Batanov G M et al 1996 Plasma formation during solid-body irradiation by microwaves and its application for localizing the energy input *J. Phys. D: Appl. Phys.* **29** 1641–8
- [31] Batanov G M, Berezhetskaya N K, Kossyi I A, Magunov A N and Silakov V P 2004 Interaction of high-power microwave beams with metal-dielectric media *Eur. Phys. J. Appl. Phys.* **26** 11–16
- [32] Kryazhev A, Buyanova M, Semenov V, Anderson D, Lisak M, Puech J, Lapiere L and Sombrin J 2002 Hybrid resonant modes of two-sided multipactor and transition to the polyphase regime *Phys. Plasmas* **9** 4736–43
- [33] Udiljak R, Anderson D, Lisak M, Semenov V E and Puech J 2007 Multipactor in a coaxial transmission line: II. Particle-in-cell simulations *Phys. Plasmas* **14** 033509
- [34] Vaughan J R M 1989 A new formula for secondary emission yield *IEEE Trans. Electron Devices* **36** 1963–7
- [35] Udiljak R, Anderson D, Lisak M, Semenov V E and Puech J 2007 Multipactor in a coaxial transmission line: I. Analytical study *Phys. Plasmas* **14** 033508
- [36] Sakamoto K, Ikeda Y and Imai T 1989 Numerical study of RF discharge caused by secondary electron emission *J. Phys. D: Appl. Phys.* **22** 1840–7